Korean J. Chem. Eng., 34(3), 876-884 (2017)
DOI: 10.1007/s11814-016-0300-6

pISSN: 0256-1115
eISSN: 1975-7220

Improvement of methane uptake inside graphene sheets using nitrogen, boron and lithium-doped structures: A hybrid molecular simulation

Atieh Hassani, Mohammad Taghi Hamed Mosavian, Ali Ahmadpour, and Nafiseh Farhadian†

Chemical Engineering Department, Faculty of Engineering, Ferdowsi University of Mashhad, Mashhad 9177948974, Iran
(*Received 29 May 2016 • accepted 24 October 2016*)

Abstract−We investigated the storage capacity of methane on the pristine and doped graphene sheets using hybrid molecular dynamics - grand canonical Monte Carlo simulation method. Methane adsorption on two parallel graphene sheets with various distances was estimated at various pressures. According to the isotherm curves, the maximum amount of adsorbed methane was observed for graphene sheets with a distance layer of 1.2 nm. This optimum structure was further doped separately with lithium, nitrogen and boron atoms in various atomic percentages to examine methane storage contents. Results showed that lithium and nitrogen-doped graphene sheets could enhance the methane storage capacity of graphene sheets whereas boron did not have any significant effect on the methane uptake. The minimum content of dopant atoms for lithium and nitrogen was estimated as 1/12 (lithium atoms/carbon atoms) and 18.5 atomic percentage, respectively, to meet new DOE's target for methane uptake.

Keywords: Methane Storage, Graphene Sheets, Doping, Hybrid Simulation, DOE Target

INTRODUCTION

Non-petroleum sources of energy that can offer energy security and environmental safety are the priority of the U.S. Department of Energy (DOE) for substitutes for fossil fuels [1]. The amount of DOE's target for methane storage capacity has progressed in the past decades, varying in the range of 150 (v(STP)/v) in 1993, 180 (v(STP)/v) in 2000 and 263 (v(STP)/v) in 2015. The recently proposed value for DOE's target is clearly higher than the previous target [1-3]. The DOE's target can be met using natural gas. It offers a renewable and clean source of energy for vehicles instead of conventional fuels such as diesel and gasoline. Natural gas is a homogeneous mixture of variable hydrocarbons, mainly methane, with environmental and economic advantages [4-10]. Methane can be a good alternative to fossil fuels due to its high energy intensity and low harmful materials like carbon dioxide, which is produced during the combustion process [11-14]. Providing suitable conditions for the storage and transportation of methane at high pressure and low temperature hampers its widespread usage [11]. Compressed natural gas (CNG) and liquid natural gas (LNG) are two commonly used methods of transporting natural gas, with a number of deficiencies such as safety issues and high cost [15,16]. Adsorbed natural gas (ANG), which can be conveniently stored at room temperature and low pressure, is an alternative procedure that can overcome these problems [15,17,18]. This technique demands appropriate adsorbents with low expense, high gas storage and good structural properties [19]. Porous carbon materials such as activated carbon [20-24], graphene sheet [25-27], pillared graphene [28,29] and carbon nanotube [27,30-32] are suitable for this purpose.

Graphene is a macromolecule with two-dimensional structures consisting of carbon atoms, with a covalent bond that can create a honeycomb lattice. Due to this special structure, graphene is characterized by numerous interesting properties such as high chemical and mechanical stability, large surface area and high electrical and thermal conductivity [27,33-38]. Because of these distinguishing features, graphene is used in different fields such as gas sensor [39], fuel cell [40], gas storage and adsorption [19]. In spite of large specific surface area and pore volume of graphene sheet related medium in comparison with some other carbon nanostructure [38], the use of carbon nanostructure in the case of gas adsorbent requires surface modification. Functionalization and doping can improve binding or adsorption strength between pristine graphene and gas molecule [2].

The doping of graphene sheet with heteroatoms like lithium, nitrogen and boron can enhance the gas storage capacity of carbon adsorbents due to the modified electronic structure [41-44]. Lithium cation generates a powerful affinity between gas molecules and adsorbents as a result of the induced dipole interaction and London dispersion which enhances the adsorption capacity [19, 45,46]. Also, by applying this cation the essential time to achieve the saturation pressure of adsorbents considerably decreases [47]. In some carbon nanostructure materials, such as different forms of covalent organic frameworks (COFs) and multilayer graphene nanostructure, the application of lithium doping for methane uptake was investigated theoretically with grand canonical Monte Carlo (GCMC) method [19,45,46]. The results showed that lithium doped COFs enhanced the methane adsorption capacity [45] even up to two times in comparison to the pristine form at lower temperature and pressure [46]. Also, Li doping increased the strength of methane adsorption on multilayer graphene sheets [19].

Nitrogen and boron doping increase the chemical reactivity of inert carbon nanostructure and the enthalpy of adsorption, leading

†To whom correspondence should be addressed.
E-mail: n.farhadian@um.ac.ir, na.farhadian@gmail.com

to the addition of extra electronic states around the Fermi level [48-51]. According to a DFT study, boron doping can lead to the physical adsorption of gases such as methane [50]. Having greater chemical reactivity of nitrogen doped compared to pure graphene sheet, comes into existence with the facile excitation of electron from valence bands to conduction bands [48]. In a recent DFT study via Vienna, *ab initio* method showed that adding nitrogen to the graphene structure could stimulate the methane uptake capacity [42]. According to our knowledge, methane uptake on the doped graphene sheets with N and B has not been reported in large scale.

Above literature review shows that in several experimental studies, lithium, nitrogen and boron-doped graphene sheets with various dopant percentages have been prepared [see Table 1], but it has not been examined for methane storage. Furthermore, there is no theoretical study underlying methane storage on doped graphene sheets with various percentage of dopant of ad atoms. The main purpose of this study was to apply doped-graphene sheets for methane storage using a theoretical method. To achieve this aim, first the best structure of pristine graphene sheets should be selected. To do so, hybrid molecular dynamics - grand canonical Monte Carlo (MD-MC) simulation - is applied to investigate the effect of distance between two parallel graphene sheets on methane storage capacity. The optimum distance is then selected for lithium, nitrogen and boron doping. Afterwards, the same simulation method is used to examine the impact of various dopant atom types and their percentages on the methane adsorption capacity. In all steps, isotherm curves are plotted and compared to each other. Finally, all structures (from dopant type and percentage) are applied to examine their ability for new DOE's targets. This is the first theoretical study that investigates the impact of dopant on the grapghene sheets for methane uptake in details using a hybrid MC-MD simulation method.

SYSTEM CONFIGURATIONS AND COMPUTATIONAL DETAILS

1. System Configurations

To perform hybrid simulations, it is necessary to construct the graphene sheet structures. The pristine graphene sheets are collected from two parallel graphene sheets with a length and width of 10 and 6 nm, respectively (Fig. 1). To calculate the optimum distance between graphene sheets for maximum methane adsorption capacity, three distances of 0.8 nm, 1.2 nm and 1.75 nm were selected (Fig. 2(a)-(c)). These values were derived from the literature based on their suggested data [19,28]. Isotherm curves were plotted for all three structures to select the optimum layer distance for the maximum methane adsorption capacity.

In the subsequent step, the optimum structure was doped with

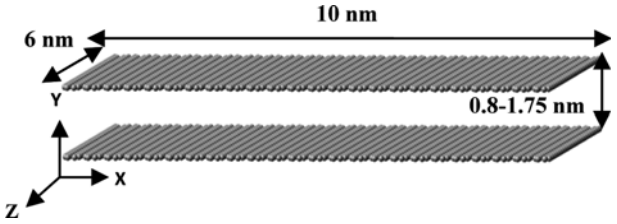

Fig. 1. Schematic of two pristine parallel graphene sheets.

lithium, nitrogen and boron separately. Moreover, for each configuration, various atomic percentages of dopant atoms were applied. Nitrogen and boron atoms were randomly placed in the hexagonal ring of carbon atoms in graphene sheets with a graphitic structure [52,53]. Boron and nitrogen atoms can be situated in graphene network in graphitic, pyridinic, pirrolic and so on. At temperatures higher than 800 °C, graphitic substitutions of N and B are more stable structures compared to other substitution forms. In other words, other substitution forms (pyridinic, pyrrolic and other) in high temperature are converted to this stable species [44,54-56]. So, in this study, graphitic substitution was selected for both N and B doping. According to DFT studies results in our previous work [57], after substitution of N and B atoms in the graphene sheet, no significant change in bond lengths and angles as well as no obvious deformation in the graphene structure were observed. Indeed, to prepare N and B doped graphene sheets, C atom was replaced with N or B without any changing of the bond length. Since the distance variances among C-N and C-B with C-C bond (C-C bond distance: 0.142 in a pristine graphene sheet) are 0.002 and 0.007 nm, so this slight diversity has insignificant effect on mass of adsorbed gas and is negligible [54]. This is another assumption in this work. Lithium atom was positioned at a distance of about 2 Å from graphene sheets [43,58]. The values for doping percentage were derived from previous theoretical and experimental studies. Table 1 shows brief arrangements of dopant percentage derived from the literature.

According to the experimental data, a graphene sheet can be doped with nitrogen, ranging from low values [65] to high atomic percentage [61]. Thus, nitrogen atomic percentages of 3.8 [36], 11.6 [63], 18.5 [61] and 23 were selected for simulation. As for boron, 1 [56], 3.8 [68], 7.6 [66] and 11.6 values were used for doping due to practical series in the experimental data. The highest doping level of nitrogen (23%) and boron (11.6%), though not observed in experiments, was selected for extra evaluation. Different atomic percentages of lithium dopant were determined from the theoretical and experimental works [43,59,72]. For lithium doping, then, it will be possible to make lithium clustering on the graphene structure. So, the selection amounts of the lithium atoms

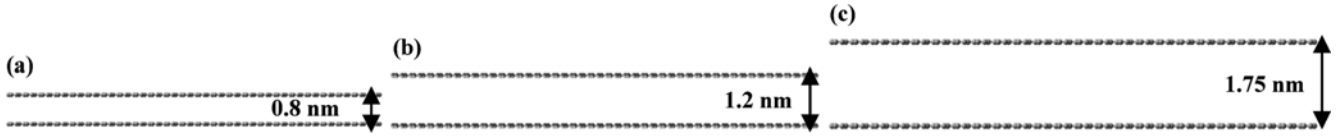

Fig. 2. Schematic of the primary structures of two parallel graphene sheets with different layer distances (a) 0.8 nm, (b) 1.2 nm, and (c) 1.75 nm.

Table 1. Different atomic contents of nitrogen, boron and lithium-doped graphene

Doped element	Methods	Atomic content	Reference
Lithium	Theoretical (DFT method)	<1/6 (Li/C)	[43]
	Lithium intercalation	<1/6 (Li/C)	[59]
Nitrogen	Microwave Irradiation	4-8.1	[33]
	Pyrolysis	16.75	[60]
	Nano-CaCO3 as template, graphitization catalyst and activating agent	18.47	[61]
	Reduction of Graphene Oxide	3-5	[36]
	Three-step wet-chemical method	8.6	[62]
	Pyrolysis	6.91-11.81	[63]
	Thermal chemical vapour deposition	0-16	[35]
	Solvothermal Synthesis	4.5-16.4	[64]
	CVD	2.1-5.6	[65]
Boron	Simple thermal annealing	7.48	[66]
		1.4	[67]
		3.45	[68]
		1.8	[69]
	Facile thermal solid-state reaction of graphene oxide with boric acid	0.57-1.92	[56]
	Catalyst-free thermal annealing approach in the presence of boron oxide	3.2	[70]
		5.93	[71]
	Pyrolysis synthesis	4.7	[55]

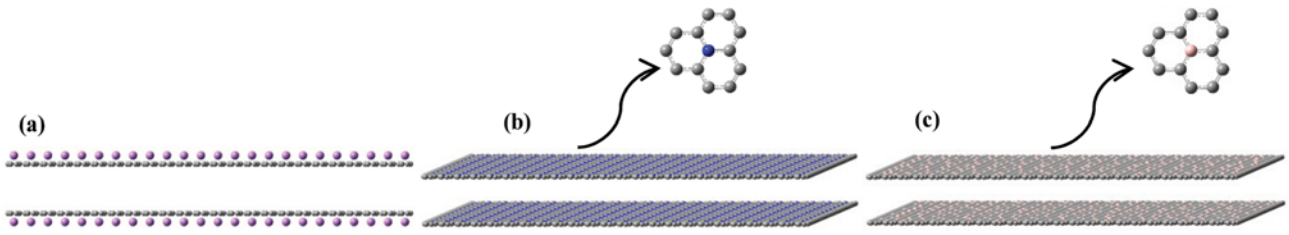

Fig. 3. Schematic of the primary structures of doped parallel graphene sheets (a) lithium, (b) nitrogen and (c) boron (color key: grey=carbon, purple=lithium, blue=nitrogen, pink=boron).

in any fix or flexible simulated structure were based on that any lithium clustering does not happen. According to the previous studies, lithium clustering may happen in ratios of 1/3 or 1/1 for Li/C [43,73]. So, for prevention of Li clustering, the maximum selected value for Li/C ratio in this study is 1/6, which is a safe amount. Accordingly, the Li/C content ratios of 1/6, 1/12 and 1/24 were selected for doping. In addition, previous DFT studies, [19, 43,57] showed that after doping the nanostructure with lithium atom, no considerable change in nanostructure shape was observed.

The simulation box was made of a cubic form (14 nm×10 nm× 10 nm). Fig. 3 shows system configurations for lithium, nitrogen and boron-doped graphene sheets.

2. Simulation Method

To determine the methane uptake capacity and adsorption isotherms, the hybrid molecular dynamics - grand canonical Monte Carlo (MD-MC) simulation, was employed. This method, based on the GCMC, uses MD algorithm for simulating atom movements, which was described completely in our previous study [28]. In a brief description, simulations were performed for pressures in the range of 1-44 bar. To maintain the balance between adsorbate and bulk phase of mentioned structure at a constant pressure, two control volumes (CVs) were placed on the top and bottom of each configuration (Fig. 4).

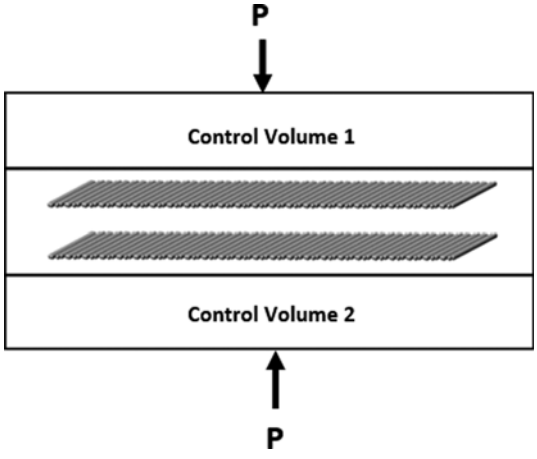

Fig. 4. Constant pressure conserved throughout the simulated configurations.

By an MC procedure, insertion-deletion process, the densities

of CVs are held steady according to Eqs. (1) and (2):

$$p^{+}=\min\left[1,\frac{Z_i V}{N_i+1}\exp(-\Delta U^{+}/k_B T)\right] \quad (1)$$

$$p^{-}=\min\left[1,\frac{N_i}{Z_i V}\exp(-\Delta U^{-}/k_B T)\right] \quad (2)$$

Here, $\Delta U^{\pm}$ are potential energy variants caused by adding or removal of one molecule, Z_i is the absolute fugacity at temperature T, V is the volume of CVs, N_i is the number of atoms of gas and Boltzmann's constant defined by k_B. The compressibility factor of methane gas was used to convert fugacity to pressure. Presumed time interval (Δt) for addition and elimination of sequential processes was 50 to 150 ps. Berendsen thermostat was applied to maintain a constant temperature of 298 K. Graphene sheets were maintained frozen in all directions during the simulation. LINCS algorithm and Leapfrog integration were used to demonstrate the physical constraints of the molecules and compute Newton's equation of motion, respectively. To keep the pressure or chemical potentials in the control volume of simulation constant, the Nosé-Hoover-Langevin piston was used [74]. All simulations were performed for 3 ns. MD simulations and visualizations were performed by Gromacs software [75] and VMD package version 1.9.1 [76], respectively.

In all simulations, graphene sheets were assumed fixed. The kinetic diameter of methane molecules as diffusive species is 0.3758 nm [2], which is smaller than the assumed distance between two graphene sheets (0.8 nm<d<1.75 nm) in this study. According to previous studies [42], at these cases, rigid or flexible structure of the adsorbents does not have any significant effect on the gas diffusivities and adsorption amounts. Moreover, there are some limitations about time of the MD simulation, which will be more noticeable in flexible structures. So, considering rigid structure is a common practice in molecular simulations of fluids [77]. Also, the methane molecule was assumed as a sphere with zero net charge. In addition, graphene sheets in the pristine and doped-configurations were assumed neutral [47,54]. Therefore, only 6-12 Lennard-Jones (LJ) potential was applied to the force field (Eq. (3)-(5)). Lorentz-Berthelot rules were also employed for calculation of intermolecular forces between methane molecules and graphene sheets as Eqs. (6), (7).

$$V_{LJ(r)}=\frac{c_{ij}^{12}}{r_{ij}^{12}}-\frac{c_{ij}^{6}}{r_{ij}^{6}} \quad (3)$$

$$c_{ij}^{12}=4\varepsilon_{ij}(\sigma_{ij})^{12} \quad (4)$$

$$c_{ij}^{6}=4\varepsilon_{ij}(\sigma_{ij})^{6} \quad (5)$$

$$\sigma_{ij}=\frac{1}{2}(\sigma_{ii}+\sigma_{jj}) \quad (6)$$

$$\varepsilon_{ij}=(\varepsilon_{ii}\varepsilon_{jj})^{1/2} \quad (7)$$

where r_{ii} is the distance between the particles, σ_{ij} and ε_{ij} are the Lennard-Jones size and energy parameters, respectively. Applied Lennard-Jones parameters are shown in Table 2. In accordance with the literature review, there are large variances of data for Lennard Jones parameters of lithium atom [78-85]. In this study, the LJ parameters for lithium atom from reference [78] were applied.

Table 2. Lennard Jones parameters for different interactions of intermolecular pairs

PAIR	C6 ($kJmol^{-1}nm^{6}$)	C12 ($kJmol^{-1}nm^{12}$)	Reference
CH_4-CH_4	0.015	4.6E-05	[86]
C-C	0.23402E-02	0.33740E-05	[75]
N-N	0.24362E-02	0.16924E-05	[75]
Li-Li	0.33231E-04	0.10554E-10	[78]
B-B	0.269239E-02	0.456371E-05	[80]

RESULTS AND DISCUSSION

1. Methane Adsorption on Pristine Graphene Sheets

At first, it is necessary to check the accuracy of the applied method for methane uptake on graphene sheets in whole range of the pressure. This was done in our previous work [28] where we compared the quantities of methane adsorption on graphene sheets with the similar theoretical and experimental studies. Our obtained results were in good conformity with previous studies that relied on the validity of the suggested method.

To choose the optimal structure for the layers distance and examine its effect on the adsorption capacity of methane, it is essential to plot the isotherm curves for pristine structure in three different distances (0.8, 1.2 and 1.75 nm).

In Fig. 5, the isotherm curves for all structures are shown and Fig. 6 depicts the schematic of methane adsorption for all structures after simulation.

As shown in Fig. 5, the maximum adsorption of methane was obtained in 1.2 nm layer space. At lower pressure (<3 bar), there is not any significant difference between the adsorption amounts of methane for various layer distances. At the pressure range of 3-10 bar, the greatest adsorption amount of methane for layer distances of 0.8 nm was achieved. By increasing the pressure up to 44 bar, however, the maximum methane adsorption was derived at a distance of 1.2 nm. Moreover, the adsorption amount of methane at the layer distance of 1.75 nm was found to be lower than

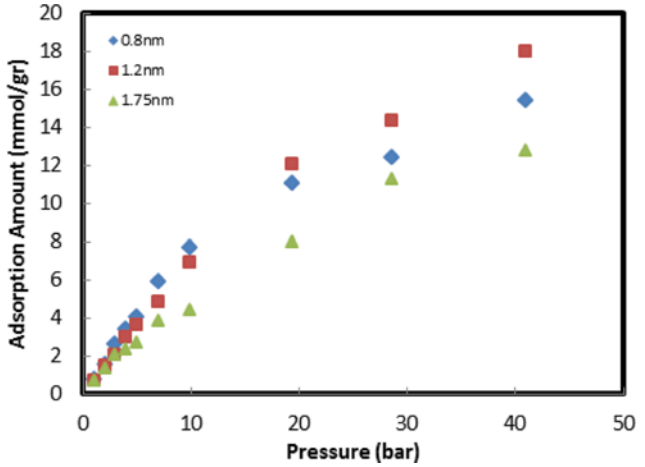

Fig. 5. Adsorption isotherm curves of pristine graphene sheets for various layer spacing.

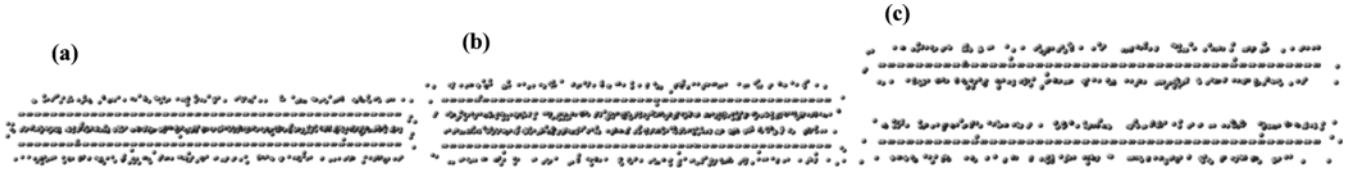

Fig. 6. Snapshots of methane adsorption at a pressure of 44 bars and a temperature of 298 K for two parallel pristine graphene sheets with various layer spacing (a) 0.8 nm, (b) 1.2 nm, and (c) 1.75 nm.

other distances in all pressure ranges. Further, Fig. 6 shows that for graphene sheets with a layer space of 0.8 nm, only one adsorbed methane layer is formed between graphene sheets, whereas it increased to two layers at higher distances. Thus, at lower distance of the graphene sheets (d≤0.8 nm), the restricted space between two graphene layers of methane adsorption leads to the formation of one adsorbed methane layer. At lower pressure (P<10 bar), methane molecules can be adsorbed with higher forces from both graphene sheets, thereby enhancing the adsorbed methane compared to other structures. With an increase in the pressure (P>10 bar), the space for extra adsorption of methane is limited, leading to a decline in the slope of isotherm curve. At a distance of 1.2 nm, two clear adsorbed layers of methane can be developed between graphene sheets. It increases the adsorption of methane in comparison to a layer space of 0.8 nm at higher pressure (P>10 bar).

At distances greater than 1.2 nm, the density of adsorbed methane layers decreases due to the weak strength of van der Waals forces between graphene sheets and methane molecules due to physical adsorption [87]. In this case, methane molecules can move freely by increasing the interlayer distance [19], thereby reducing the total amounts of adsorbed methane. Finally, 1.2 nm layer distance of graphene sheet was assumed as the optimum to obtain the maximum methane adsorption, especially at higher pressures.

2. Methane Adsorption on Doped Graphene Sheets

After determining the optimum structure of two graphene sheets, the effect of doping-related factors such as the type of dopant and doping percentage on the methane adsorption was investigated. Lithium, nitrogen and boron were selected as adatoms, and vari-

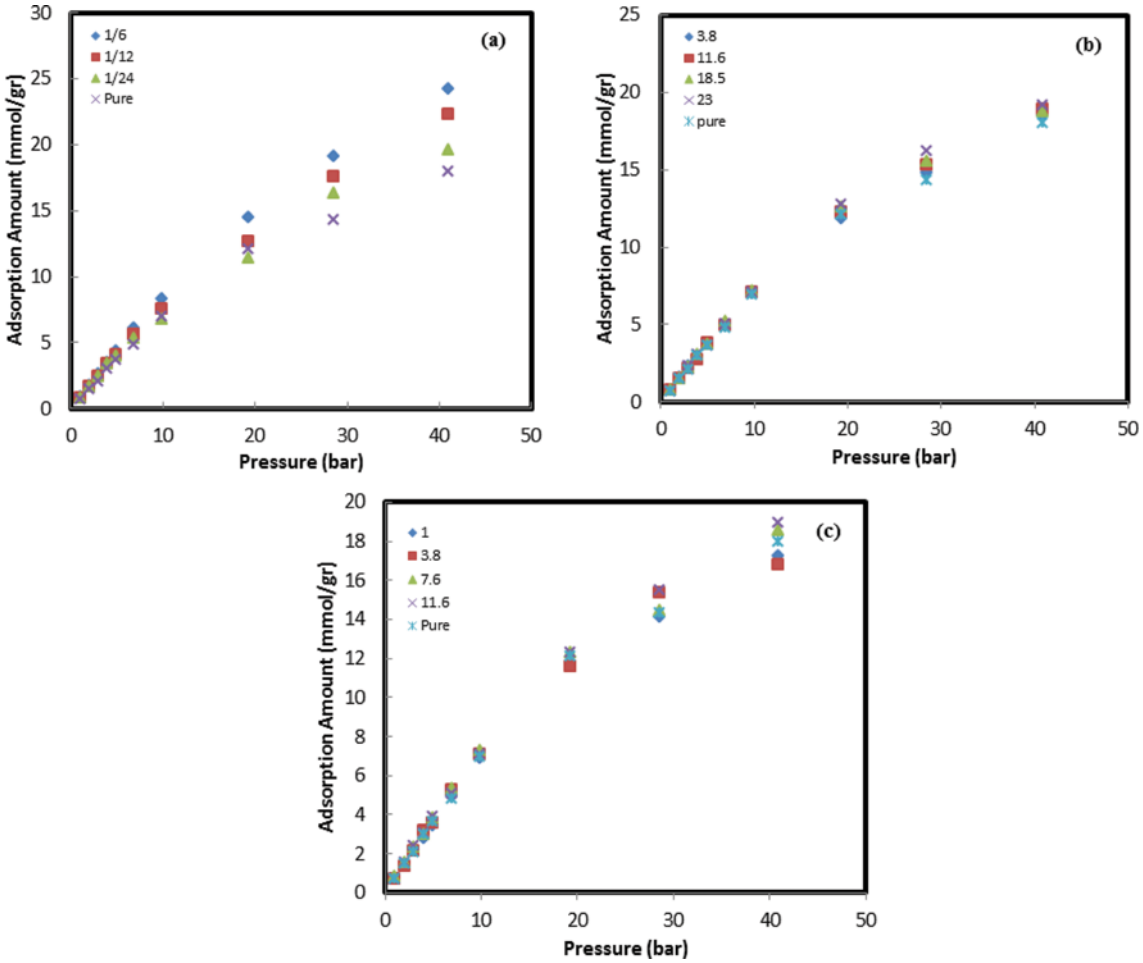

Fig. 7. Isotherm curves of methane adsorption in (a) lithium, (b) nitrogen and (c) boron-doped graphene sheets.

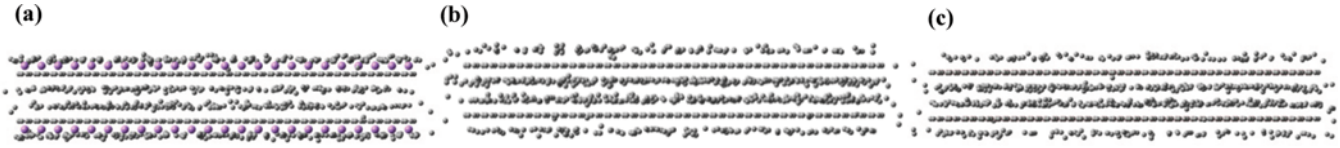

Fig. 8. Snapshots of graphene sheets after methane adsorption at a pressure of 44 bars and a temperature of 298 K for (a) lithium-doped, (b) nitrogen-doped and (c) boron-doped structures.

ous dopant percentages of Li, N and B were added to the graphene structures. The isotherm curves for all doped structures were plotted following the simulations (Fig. 7). In Fig. 8, a schematic of the doped graphene structures is shown after the methane adsorption at a pressure of 44 bar.

According to the isotherm curves, the doping of graphene sheets with lithium atom at various doping percentages and pressures lower than 5 bar did not have any significant effect on the adsorption capacity. In the same way, this behavior was observed for nitrogen atom at a pressure of 20 bar and lower values. An increase in the pressure and dopant percentage can enhance methane adsorption uptake. Overall, the results suggest that lithium, as an adatom, has the greatest impact on the methane adsorption capacity. Furthermore, the effect of dopant percentage variation of lithium-doped structure on the adsorbent capacity is greater than boron and nitrogen-doped graphene sheets. However, boron-doping did not have any specific effect on the methane adsorption.

A scanning of the snapshots of doped structures (Fig. 8(a)-(c)) after methane adsorption revealed the formation of four dense graphene layers inside and outside graphene sheets in all systems. Methane molecules are located at various distances from graphene sheets due to various interactions between dopant atoms and adsorbed gas molecules. The distance of methane molecules from the graphene sheet is smallest in the lithium-doped configuration and largest in the boron-doped pattern. This observation can be confirmed by radial distribution function (RDF) curves (Fig. 9(a)). In a system of particles, RDF describes the density variable as a function of the distance from a reference particle. According to the RDF curves, the first peak of methane molecules and graphene sheets is observed at the closer distance of lithium-doped structures with the highest height. It is then followed by the first peak of RDF curve of nitrogen and boron-doped structures. This is due to the strength of interactions between methane molecules and dopant atoms of the graphene sheets.

As shown in Fig. 9(b), since lithium has the highest RDF peak, the maximum methane adsorption occurs in the lithium-doped graphene sheet structures.

Moreover, in accordance with the simulation results, at approximately the same doping percentage of Li, N and B at both lower (Li/C=1/24≅4.16% and 3.8% N and B doped (Fig. 10(a))) and higher (Li/C=1/12≅8.3% and 11.6% N and B doped (Fig. 10(b))) values, no considerable differences were observed between adsorption amounts of methane in all doped structures, specially at a pressure lower than 20 bar. By enhancing the pressure upper than 20 bar, although the adsorption amounts of methane differs for various doped structures, this difference is not noticeable at lower doping percentage. As doping percentage increases, the adsorption amounts of methane on the Li doped structure become higher. In

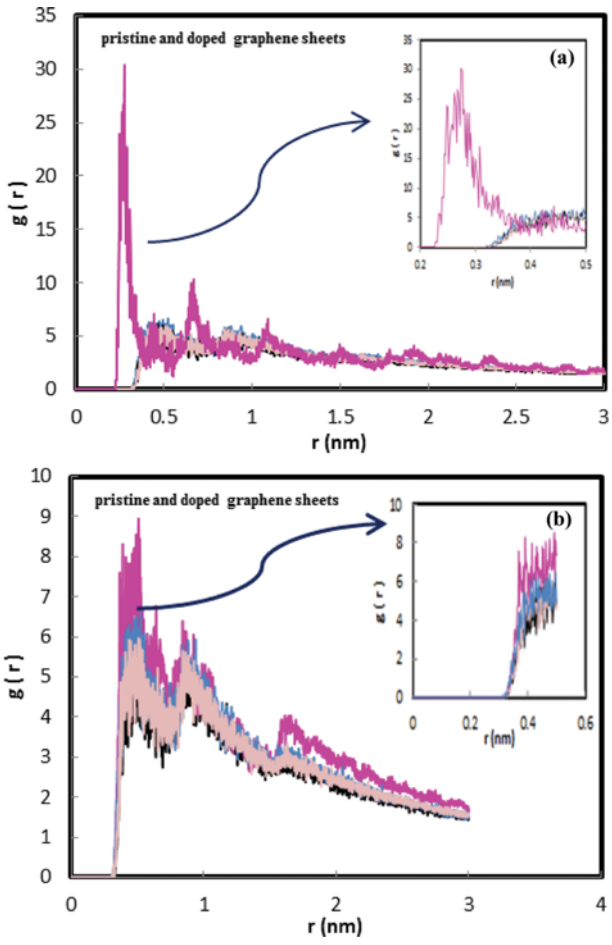

Fig. 9. RDF curves for pristine, lithium-doped, nitrogen-doped and boron-doped graphene sheets between (a) methane molecules and doped atoms and (b) methane molecules and graphene sheets (Color key: black=carbon, purple=lithium, blue=nitrogen, pink=boron).

summary, it could be concluded that Li doped structure has the greatest effect on the methane adsorption. In other words, it is possible to obtain the determined values of adsorbed methane at lower Li doping ratio in comparison to N and B doped structures.

3. DOE Target

Recently, the U.S. Department of Energy set a new value of 263 V (STP)/V (at standard temperature of 298 K, a pressure of 1.01 bar, and an equivalent volume of methane per volume of the adsorbent material) for methane storage in ambient temperature at a pressure of 35 bar [2]. All calculated isotherm curves were plotted in accordance with this definition and compared to DOE's target (Fig. 11). The results showed that lithium and nitrogen-

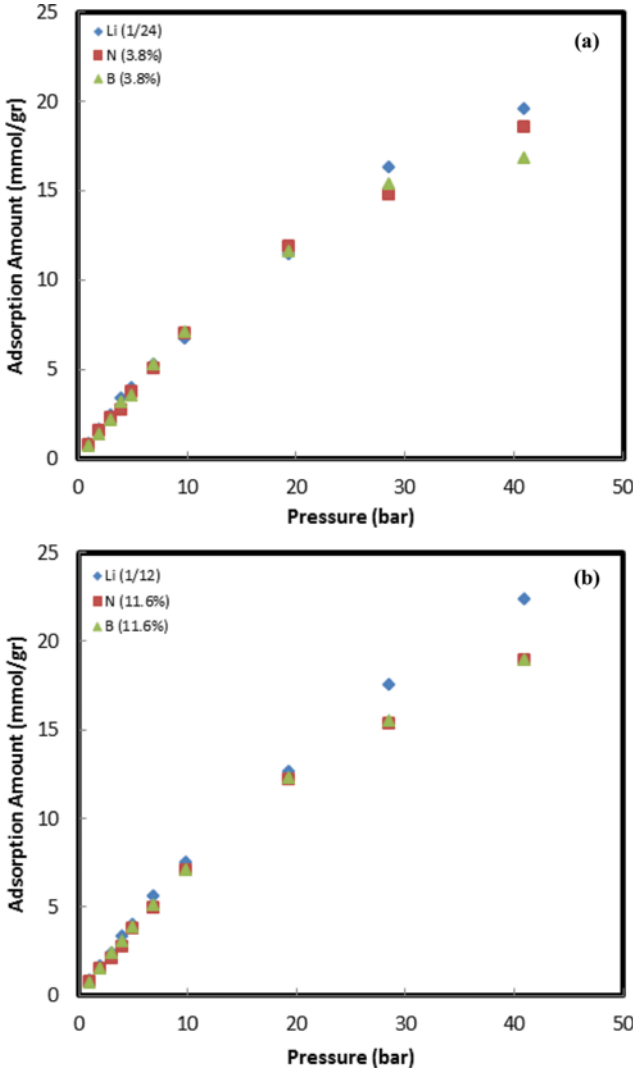

Fig. 10. Isotherm curves of methane adsorption in doped graphene sheets at (a) lower (Li/C=1/24 and 3.8% N and B doped percentage) and (b) higher (Li/C=1/12 and 11.6% N and B doped) doped percentage.

doped graphene sheets with higher dopant content (1/6 and 1/12 of Li/C for lithium-doped and 18.5 and 23% for nitrogen-doped) could meet DOE's new target. All other configurations, nonetheless, were helpful structures for passing the old DOE target (180 V (STP)/V) [3].

Note that the calculated values for DOE's target in Li-doped graphene sheets is in agreement with previous study performed with GCMC method [19]. Since, there are wide ranges for Li-C LJ parameters; this could confirm the accuracy of applied LJ parameters in this study.

CONCLUSIONS

We examined the ability of graphene sheets in pristine and doped forms for methane storage. Hybrid molecular dynamics-Monte Carlo simulation method was used. In the first step, the optimal layer distances between two graphene sheets were determined to

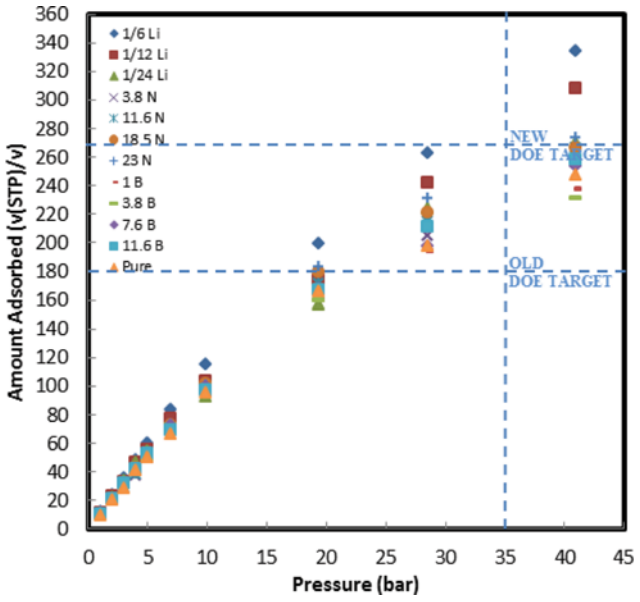

Fig. 11. Comparison of adsorbed methane molecules (V (STP)/V) on the pristine and doped graphene sheets with various dopant percentages at a temperature of 298 K.

achieve the maximum methane adsorption capacity. According to the simulation results and isotherm parameters, a layer distance of 1.2 nm was selected as an optimum structure of graphene sheets. Then, the impact of lithium, nitrogen and boron doping on the optimum configuration of methane appealing capacity was studied. The results showed that lithium and nitrogen-doped graphene sheets could enhance methane adsorption capacity in comparison to pristine pattern, whereas boron-doped structure did not have any significant effect on methane adsorption. Finally, doped-graphene sheets with a dopant value of 1/6 and 1/12 for lithium and 18.5 and 23% for nitrogen were selected as adsorbent that could meet new DOE's target. One of the main points in applying doped graphene sheets in vehicles is the desorption process. Li doped graphene sheets could enhance methane adsorption capacity significantly, but practically, desorption of methane from this structure may be harder than the others. Similar phenomenon has been reported before [42]. Refer to our previous study about methane adsorption energy on the pristine and doped graphene sheets; it was observed that Li-doping enhances the methane adsorption energy up to about seven -fold in comparison to pristine structure due to stronger physisorption attachment [57]. So, it is necessary to perform additional studies about the desorption process from these materials.

REFERENCES

1. T. Düren, L. Sarkisov, O. M. Yaghi and R. Q. Snurr, *Langmuir*, **20**, 2683 (2004).
2. S. Gadipelli and Z. X. Guo, *Prog. Mater. Sci.*, **69**, 1 (2015).
3. T. Burchell and M. Rogers. SAE Technical Paper (2000).
4. S. Cavenati, C. A. Grande and A. E. Rodrigues, *J. Chem. Eng. Data*, **49**, 1095 (2004).

5. J. L. Vicente and A. G. Albesa. Description of Adsorbed Phases on Carbon Surfaces: A Comparative Study of Several Graphene Models, INTECH Open Access Publisher (2011).
6. C. Solar, A. G. Blanco, A. Vallone and K. Sapag, Natural Gas 205 (2010).
7. M. Sudibandriyo, *Int. J. Eng. Technol.*, **11**, 86 (2011).
8. Y. Wang, M. Hashim, C. Ercan, A. Khawajah and R. Othman, 21st Annual Saudi-Japan Symposium, November (2011).
9. P. A. Denis, *Chem. Phys.*, **353**, 79 (2008).
10. M. Yamamoto, T. Itoh, H. Sakamoto, T. Fujimori, K. Urita, Y. Hattori, T. Ohba, H. Kagita, H. Kanoh and S. Niimura, *Adsorption*, **17**, 643 (2011).
11. P. Kowalczyk, L. Solarz, D. Do, A. Samborski and J. MacElroy, *Langmuir*, **22**, 9035 (2006).
12. A. Yamashita, Y. Mori, T. Oshima and Y. Baba, *Carbon*, **76**, 469 (2014).
13. S. Takenaka, Y. Shigeta and K. Otsuka, *Chem. Lett.*, **32**, 26 (2003).
14. J. Kim, A. Maiti, L.-C. Lin, J. K. Stolaroff, B. Smit and R. D. Aines, *Nat. Commun.*, **4**, 1694 (2013).
15. D. A. Gómez-Gualdrón, C. E. Wilmer, O. K. Farha, J. T. Hupp and R. Q. Snurr, *J. Phys. Chem. C.*, **118**, 6941 (2014).
16. S. L. Candelaria, Y. Shao, W. Zhou, X. Li, J. Xiao, J.-G. Zhang, Y. Wang, J. Liu, J. Li and G. Cao, *Nano Energy*, **1**, 195 (2012).
17. D. Lozano-Castello, J. Alcaniz-Monge, M. De la Casa-Lillo, D. Cazorla-Amorós and A. Linares-Solano, *Fuel*, **81**, 1777 (2002).
18. M. Khorashadizadeh, M. N. Shahrak and A. Shahsavand, *Korean J. Chem. Eng.*, **31**, 1994 (2014).
19. J.-J. Chen, W.-W. Li, X.-L. Li and H.-Q. Yu, *Environ. Sci. Technol.*, **46**, 10341 (2012).
20. Y. Wang, C. Ercan, A. Khawajah and R. Othman, *AIChE J.*, **58**, 782 (2012).
21. R. Heller and M. Zoback, *Journal of Unconventional Oil and Gas Resources*, **8**, 14 (2014).
22. L. Giraldo and J. C. Moreno-Piraján, *Mater. Sci. Appl.*, **2**, 331 (2011).
23. M. Molashahi and H. Hashemipour, *Korean J. Chem. Eng.*, **29**, 601 (2012).
24. S. S. A. Syed-Hassan and M. S. M. Zaini, *Korean J. Chem. Eng.*, 1 (2015).
25. K. Mosher, J. He, Y. Liu, E. Rupp and J. Wilcox, *Int. J. Coal Geol.*, **109**, 36 (2013).
26. W. Zhao and Q. Y. Meng. Advanced Materials Research, Trans Tech Publ (2013).
27. B.-H. Kim, G.-H. Kum and Y.-G. Seo, *Korean J. Chem. Eng.*, **20**, 104 (2003).
28. A. Hassani, M. T. H. Mosavian, A. Ahmadpour and N. Farhadian, *J. Chem. Phys.*, **142**, 234704 (2015).
29. R. Kumar, V. M. Suresh, T. K. Maji and C. Rao, *Chem. Commun.*, **50**, 2015 (2014).
30. S. Monemtabary, M. S. Niasar, M. Jahanshahi and A. A. Ghoreyshi, *System*, **2**, 17 (2013).
31. M. Rasoolzadeh, S. Fatemi, M. Gholamhosseini and M. A. Moosaviyan, *Iran J. Chem. Chem. Eng.*, **27** (2008).
32. X. Zhang and W. Wang, *Fluid Phase Equilib.*, **194**, 289 (2002).
33. K. H. Lee, J. Oh, J. G. Son, H. Kim and S.-S. Lee, *ACS Appl. Mater. Interfaces*, **6**, 6361 (2014).
34. L. Wang, Z. Sofer, J. Luxa and M. Pumera, *J. Mater. Chem. C.*, **2**, 2887 (2014).
35. Z. Luo, S. Lim, Z. Tian, J. Shang, L. Lai, B. MacDonald, C. Fu, Z. Shen, T. Yu and J. Lin, *J. Mater. Chem.*, **21**, 8038 (2011).
36. X. Li, H. Wang, J. T. Robinson, H. Sanchez, G. Diankov and H. Dai, *J. Am. Chem. Soc.*, **131**, 15939 (2009).
37. S. Bai and X. Shen, *RSC Adv.*, **2**, 64 (2012).
38. Z. Zhu and Q. Zheng, *Appl. Therm. Eng.*, **108**, 605 (2016).
39. J. Dai, J. Yuan and P. Giannozzi, *Appl. Phys. Lett.*, **95**, 232105 (2009).
40. L. Qu, Y. Liu, J.-B. Baek and L. Dai, *ACS Nano*, **4**, 1321 (2010).
41. K. Gopalakrishnan, K. Moses, P. Dubey and C. Rao, *J. Mol. Struct.*, **1023**, 2 (2012).
42. Y. Wang, Y. Feng, G. Meng, X. Dong and X. Huang, Phys. Status Solidi B. (2015).
43. X. Fan, W. Zheng and J.-L. Kuo, *ACS Appl. Mater. Interfaces*, **4**, 2432 (2012).
44. L. Zhao, M. Levendorf, S. Goncher, T. Schiros, L. Palova, A. Zabet-Khosousi, K. T. Rim, C. Gutierrez, D. Nordlund and C. Jaye, *Nano Lett.*, **13**, 4659 (2013).
45. Z. Yang and D. Cao, *J. Phys. Chem. C.*, **116**, 12591 (2012).
46. J. Lan, D. Cao and W. Wang, *Langmuir*, **26**, 220 (2009).
47. G. K. Dimitrakakis, E. Tylianakis and G. E. Froudakis, *Nano Lett.*, **8**, 3166 (2008).
48. P. Wu, Y. Qian, P. Du, H. Zhang and C. Cai, *J. Mater. Chem.*, **22**, 6402 (2012).
49. N. P. Stadie, California Institute of Technology, PhD (2013).
50. X.-Q. Liu, Y. Xue, Z.-Y. Tian, J.-J. Mo, N.-X. Qiu, W. Chu and H.-P. Xie, *Appl. Surf. Sci.*, **285**, 190 (2013).
51. C. Ewels, M. Glerup, V. Krstic, V. Basiu and E. Basiuk. In: Chemistry of Carbon Nanotubes, American Scientific Publishers (2007).
52. R. Lv, Q. Li, A. R. Botello-Méndez, T. Hayashi, B. Wang, A. Berkdemir, Q. Hao, A. L. Elías, R. Cruz-Silva and H. R. Gutiérrez, *Sci. Rep.*, **2** (2012).
53. H. Tachikawa, T. Iyama and K. Azumi, *Jpn. J. Appl. Phys.*, **50**, 01BJ03 (2011).
54. K. V. Kumar, K. Preuss, L. Lu, Z. X. Guo and M. M. Titirici, *J. Phys. Chem. C.*, **119**, 22310 (2015).
55. L. Niu, Z. Li, W. Hong, J. Sun, Z. Wang, L. Ma, J. Wang and S. Yang, *Electrochim. Acta*, **108**, 666 (2013).
56. X. Xu, T. Yuan, Y. Zhou, Y. Li, J. Lu, X. Tian, D. Wang and J. Wang, *Int. J. Hydrogen Energy*, **39**, 16043 (2014).
57. A. Hassani, M. T. H. Mosavian, A. Ahmadpour and N. Farhadian, *Comput. Theor. Chem.*, **1084**, 43 (2016).
58. J. Zheng, Z. Ren, P. Guo, L. Fang and J. Fan, *Appl. Surf. Sci.*, **258**, 1651 (2011).
59. W. Bao, J. Wan, X. Han, X. Cai, H. Zhu, D. Kim, D. Ma, Y. Xu, J. N. Munday and H. D. Drew, *Nat. Commun.*, **5** (2014).
60. S. Yang, X. Feng, X. Wang and K. Müllen, *Angew. Chem. Int. Ed.*, **50**, 5339 (2011).
61. G. Yang, H. Han, T. Li and C. Du, *Carbon*, **50**, 3753 (2012).
62. D. Yu, L. Wei, W. Jiang, H. Wang, B. Sun, Q. Zhang, K. Goh, R. Si and Y. Chen, *Nanoscale*, **5**, 3457 (2013).
63. M. Zhou, X. Li, J. Cui, T. Liu, T. Cai, H. Zhang and S. Guan, *Int. J. Electrochem. Sci.*, **7**, 9984 (2012).
64. D. Deng, X. Pan, L. Yu, Y. Cui, Y. Jiang, J. Qi, W.-X. Li, Q. Fu, X. Ma and Q. Xue, *Chem. Mater.*, **23**, 1188 (2011).
65. Y.-F. Lu, S.-T. Lo, J.-C. Lin, W. Zhang, J.-Y. Lu, F.-H. Liu, C.-M.

Tseng, Y.-H. Lee, C.-T. Liang and L.-J. Li, *ACS Nano*, **7**, 6522 (2013).
66. D.-Y. Yeom, W. Jeon, N. D. K. Tu, S. Y. Yeo, S.-S. Lee, B. J. Sung, H. Chang, J. A. Lim and H. Kim, *Sci. Rep.*, **5** (2015).
67. Y. Zhang, R. Sun, B. Luo and L. Wang, *Electrochim. Acta*, **156**, 228 (2015).
68. L. Zhang, Z.-Y. Zhang, R.-P. Liang, Y.-H. Li and J.-D. Qiu, *Anal. Chem.*, **86**, 4423 (2014).
69. T. Lin, F. Huang, J. Liang and Y. Wang, *Energy Environ. Sci.*, **4**, 862 (2011).
70. Z.-H. Sheng, H.-L. Gao, W.-J. Bao, F.-B. Wang and X.-H. Xia, *J. Mater. Chem.*, **22**, 390 (2012).
71. M. Sahoo, K. Sreena, B. Vinayan and S. Ramaprabhu, *Mater. Res. Bull.*, **61**, 383 (2015).
72. K. Sugawara, K. Kanetani, T. Sato and T. Takahashi, *AIP Advances*, **1**, 022103 (2011).
73. S. S. Han and S. S. Jang, *Chem. Commun.*, 5427 (2009).
74. K. Malek and M. Sahimi, *J. Chem. Phys.*, **132**, 014310 (2010).
75. D. van der Spoel, E. Lindahl, B. Hess, A. R. van Buuren, E. Apol, P. J. Meulenhoff, D. P. Tieleman, A. Sijbers, K. A. Feenstra and R. van Drunen, Gromacs User Manual (2010).
76. T. a. C. B. Group, VMD User's Guide (2012).
77. G. P. Lithoxoos, L. D. Peristeras, G. C. Boulougouris and I. G. Economou, *Mol. Phys.*, **110**, 1153 (2012).
78. J. Chandrasekhar, D. C. Spellmeyer and W. L. Jorgensen, *J. Am. Chem. Soc.*, **106**, 903 (1984).
79. Z. Peng, C. S. Ewig, M.-J. Hwang, M. Waldman and A. T. Hagler, *J. Phys. Chem. A*, **101**, 7243 (1997).
80. O. N. Kalugin, O. V. Prezhdo and V. V. Chaban, *Microscopic structure and dynamics of molecular liquids and electrolyte solutions confined by Carbon NanoTubes: Molecular dynamics simulations*, INTECH Open Access Publisher (2011).
81. A. K. Rappé, C. J. Casewit, K. Colwell, W. Goddard Iii and W. Skiff, *J. Am. Chem. Soc.*, **114**, 10024 (1992).
82. A. H. Mao and R. V. Pappu, *J. Chem. Phys.*, **137**, 064104 (2012).
83. O. N. Kalugin, A. K. Adya, M. N. Volobuev and Y. V. Kolesnik, *Phys. Chem. Chem. Phys.*, **5**, 1536 (2003).
84. V. Chaban and O. Kalugin, *J. Mol. Liq.*, **145**, 145 (2009).
85. S. S. Han, A. C. van Duin, W. A. Goddard and H. M. Lee, *J. Phys. Chem. A*, **109**, 4575 (2005).
86. F. Cuadros, I. Cachadiña and W. Ahumada, *Mol. Eng.*, **6**, 319 (1996).
87. L. Ortiz, B. Kuchta, L. Firlej, M. Roth and C. Wexler, *Mater. Res. Express*, **3**, 055011 (2016).